High-power 2.3 μm Tm:YLF laser with intracavity upconversion pumping by a Nd:ASL laser at 1051 nm

Hippolyte Dupont, Timothée Lenfant, Lauren Guillemot, Pavel Loiko, Xavier Delen, Pascal Loiseau, Bruno Viana, Thierry Georges, Patrick Georges, Patrice Camy, et al.

High-power 2.3 µm Tm:YLF laser with intracavity upconversion pumping by a Nd:ASL laser at 1051 nm

Hippolyte Dupont,[1] Timothée Lenfant,[1] Lauren Guillemot,[2] Pavel Loiko,[2] Xavier Delen,[1] Pascal Loiseau,[3] Bruno Viana,[3] Thierry Georges,[4] Patrick Georges,[1] Patrice Camy,[2] and Frédéric Druon[1,*]

[1]Université Paris-Saclay, Institut d'Optique Graduate School, CNRS, Laboratoire Charles Fabry, 91127 Palaiseau, France
[2]Centre de Recherche sur les Ions, les Matériaux et la Photonique (CIMAP), UMR 6252 CEA-CNRS-ENSICAEN, Université de Caen, 6 Boulevard Maréchal Juin, 14050 Caen Cedex 4, France
[3]Chimie ParisTech, PSL University, CNRS, Institut de Recherche de Chimie Paris, 11 rue Pierre et Marie Curie, 75005 Paris, France
[4]Oxxius S.A-4 rue Louis de Broglie 22300 Lannion, France
**frederic.druon@institutoptique.fr*

Received XX Month XXXX; revised XX Month, XXXX; accepted XX Month XXXX; posted XX Month XXXX (Doc. ID XXXXX); published XX Month XXXX

A Tm:$LiYF_4$ laser operating on the $^3H_4 \rightarrow {}^3H_5$ transition is embedded in a high-power diode-pumped Nd:ASL laser for intracavity upconversion pumping at 1.05 µm. This leads to a record-high output power at 2.3 µm for any bulk Thulium laser pumped by an upconversion process. The continuous-wave Tm:$LiYF_4$ laser delivers 1.81 W at 2.3 µm for 32 W of laser-diode pump power, making this kind of pumping competitive with direct diode pumping. The intracavity pumping process allows for counteracting the low absorption inherent to upconversion pumping and to dispatch the thermal loads on two separate laser crystals. The proposed laser architecture also features a relatively weak heating of the Tm:$LiYF_4$ crystal, and an increased tolerance to Tm^{3+} absorption. This laser design opens a new paradigm that holds great promise for high-power 2.3-µm solid-state lasers based on thulium ions.

http://dx.doi.org/10.1364/OL.99.099999

Lasers emitting within the K-band of atmosphere (at 2.1 - 2.4 µm) represent a promising domain of research, as they find applications in diverse fields such as atmosphere gas sensing, non-invasive blood glucose testing and combustion studies [1,2]. Several technologies have been employed to develop 2.3-µm laser sources, including optical parametric oscillators [3], semiconductor lasers [4,5], and solid-state lasers using Cr^{2+}:ZnS / Cr^{2+}:ZnSe as gain media [6]. Another idea to achieve laser emission at this wavelength is to exploit the $^3H_4 \rightarrow {}^3H_5$ transition of thulium ions (Tm^{3+}) [7]. In this context, Tm^{3+}-doped gain media offer a rich variety of pumping configurations. To date, direct pumping from the ground state ($^3H_6$) to the upper laser level ($^3H_4$) at 0.8 µm has demonstrated the capability to achieve both high laser slope efficiencies [8] and the generation of multi-Watt laser output power by using spatially multimode AlGaAs diode lasers as pump sources [9]. Based on the mature technology of high-power 0.8 µm AlGaAs laser diodes, Tm lasers operating either on the $^3H_4 \rightarrow {}^3H_5$ electronic transition or phonon-assisted $^3F_4 \rightarrow {}^3H_6$ transition (below 2.3 µm) accessed the highest output powers at 2.3 µm. Yu *et al.* reported on a diode-pumped Tm:$GdVO_4$ laser delivering 6.09 W at 2.29 µm [10]. Cascade laser emission on the subsequent transitions $^3H_4 \rightarrow {}^3H_5$ and $^3F_4 \rightarrow {}^3H_6$ has demonstrated advantages in some configurations [11,12].

The innovative upconversion (UC) pumping scheme at 1 µm shows great promise, leveraging the well-established Yb fiber laser, as well as Nd diode-pumped solid-state laser technologies as pump sources. As illustrated in Fig. 1(a), this pumping scheme involves a non-resonant ground state absorption (GSA, $^3H_6 \rightarrow {}^3H_5$), leading to the population of the intermediate $^3F_4$ metastable level after a non-radiative relaxation step. Subsequently, the resonant $^3F_4 \rightarrow {}^3F_{2,3}$ excited state absorption (ESA) populates the upper laser level. Additionally, an efficient cross-relaxation (CR) process, $^3H_4 + {}^3H_6 \rightarrow {}^3F_4 + {}^3F_4$, positively contributes to this excitation scheme by initiating a photon avalanche mechanism, as shown in Fig. 1(a). This CR process is more efficient than the GSA to populate the $^3F_4$ level [13-15]. UC pumping has been successfully demonstrated in Tm fiber [13] and crystalline [14] lasers at 2.3 µm. However, in the case of crystals, this pumping scheme is challenging: (i) first, the ESA peaks are typically rather narrow, and one needs to precisely adjust the pump wavelength; (ii) second, high Tm^{3+} doping levels / long crystals are required to reach sufficiently high pump absorption and (iii) high pump intensities are essential since the absorption via the UC pumping mechanism is intensity dependent. Often, for single pass pumping, the absorption saturates at 20-30%. To overcome these limitations, dual-wavelength pumping has been proposed as a solution. However, the efficiency was clearly lower than that in the case of direct pumping [15].

In the present work, we propose an innovative idea using an intracavity upconversion pumping scheme that relies on the well-developed technology of diode-pumped Nd solid-state lasers to access highly-efficient and high-brightness pumping. Considering the high gain of Nd^{3+}-doped crystals and the low absorption of Tm^{3+} ions around 1 µm, this kind of intracavity pumping is an interesting association to develop high-power and efficient laser sources at 2.3 µm being competitive with the direct diode-pumping despite a dual laser stage. Similar intracavity pumping schemes were developed for other laser transitions of rare-earth ions [16-19].

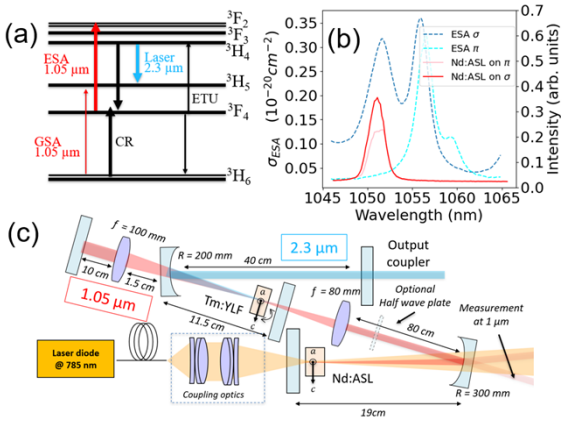

Fig. 1. (a) Energy-level scheme of thulium ions, GSA: ground-state absorption, ESA: excited-state absorption, CR: cross-relaxation, ETU: energy-transfer upconversion; (b) ESA cross-section, σ_{ESA}, for the $^3F_4 \rightarrow {}^3F_{2,3}$ transition of Tm^{3+} ions in $LiYF_4$ for π and σ light polarizations compared to the emission spectrum of the Nd:ASL laser when the Tm-crystal is oriented for pumping into π and σ polarizations; (c) Laser setup. The orientation of the Nd:ASL crystal is fixed and the Tm:$LiYF_4$ crystal can be rotated to access pumping into π or σ polarizations.

As gain materials for our proof-of-principle demonstration of the proposed intracavity upconversion pumping scheme, we used an ***a***-cut 2.5 at.% Tm^{3+}-doped $LiYF_4$ fluoride crystal (8 mm-thick) and an ***a***-cut 3 at.% Nd^{3+}-doped $Sr_{1-x}Nd_yLa_{x-y}Mg_xAl_{12-x}O_{19}$ one (strontium lanthanum aluminate, abbreviated: Nd:ASL, 10 mm-thick). This choice has been made considering the previously achieved promising performance of Tm:$LiYF_4$ under upconversion pumping [14,15] and the interesting match between the ESA spectrum of Tm^{3+} ions in $LiYF_4$ and the laser emission wavelength of Nd:ASL, namely 1051 nm, as shown in Fig. 1(a) [20,21]. The corresponding ESA cross-sections, σ_{ESA}, are 0.32×10^{-20} cm^2 for σ-polarized light and 0.04×10^{-20} cm^2 for π polarization at 1051 nm. The stimulated-emission cross section of Nd^{3+} ions in ASL is 0.32×10^{-20} cm^2 at 1051 nm for σ polarization with a strong anisotropy in favor of this principal optical direction imposing a linear laser polarization (σ). In the present experiment, the Nd:ASL crystal is wrapped with indium foil and fixed in a water-cooled copper mount kept at 18 °C. The primary pump source is a high-power fiber-coupled AlGaAs laser diode with a numerical aperture of 0.22 and a fiber core diameter of 106 µm, emitting up to 43 W at 785 nm. The Nd:ASL crystal is placed after a dichroic flat mirror in a V-shaped laser cavity designed to incorporate a second beam waist with a radius of 45 µm using two intracavity lenses, as depicted in Fig. 1(c). The Tm:$LiYF_4$ crystal is positioned at this second mode waist, where the residual pump at 0.8 µm is neglibible (<1 mW). It is also clamped between two indium sheets in a copper frame water cooled at 18 °C. We had the possibility of turning the crystal by 90° when pumping it at 1051 nm. For the 2.3 µm laser, a V-shaped cavity is implemented, consisting of two dichroic mirrors coated for high transmission at 1.05 µm and high reflectivity at 2.3 µm: a plane mirror and a concave one with a radius of curvature of -200 mm, both located within the Nd-laser cavity. The folding angle is around 5° to minimize the astigmatism. The end mirror is a plane 2.5% output coupler corresponding to the optimum 2.3-µm laser performance. The curved dichroic mirror functioned as a plano-concave lens within the Nd-laser cavity which was considered when designing the latter. Both laser crystals were anti-reflection (AR) coated at 1.05 µm. The Tm-crystal is also AR coated at 2.3 µm. Thermal lenses of both crystals are experimentally compensated by optimizing the cavities. Both 1.05 µm and 2.3 µm lasers operate on the TEM_{00} mode, see Fig. 2(d).

In this original setup, a power of 1.81 W at 2.3 µm has been achieved for a laser diode pump power of 42 W, Fig. 2. This corresponds to an intracavity power of 30 W at 1051 nm calculated based on the leakage from the first plano-concave mirror with a transmission of 0.27%, Fig. 1(c). The 1.05 µm pump radiation is linearly polarized corresponding to σ in the Tm:$LiYF_4$ crystal. The pump absorption of 1051 nm radiation in the Tm-crystal is measured to be 20% per pass. The marginal absorption for low power pumping corresponds only to the GSA when the intensity is too low to populate the $^3F_4$ level and provide strong ESA. For high power pumping, absorption saturation could be explained by CR and energy-transfer upconversion. The maximum power at 2.3 µm is limited by thermal lensing in the Nd:ASL crystal that becomes difficult to be compensated for pump powers at 0.8 µm exceeding 42 W.

However, to the best of our knowledge, this output power is record-high for any Tm laser using an upconversion pumping scheme for both crystalline and fiber geometries. For comparison, Guillemot *et al.* achieved 0.10 W at 2.30 µm by pumping a Tm:$LiYF_4$ crystal with 0.8 W of absorbed pump power at 1.04 µm [14] and Morova *et al.* reported on a Tm:KY_3F_{10} laser delivering 0.12 W at 2.34 µm for 2.36 W of incident pump power at 1.06 µm [22]. The developed laser architecture also makes it possible to obtain the highest CW output power at 2.3 µm using the Tm:$LiYF_4$ crystal, among all the pump sources applied so far. Kifle *et al.* developed a Tm:$LiYF_4$ laser pumped by a 780 nm laser diode delivering up to 2.11 W at 2.30 µm for a maximum absorbed pump power of ~10 W however in the quasi-CW regime [9]. The intracavity pumping scheme not only improves the efficiency of upconversion pumping by one order of magnitude, but also makes it clearly competitive with direct diode pumping.

From this point of view, one advantage of intracavity upconversion pumping versus direct diode pumping relies on a better and easier thermal management. The significant heating due to the high-power diode pumping is localized in the Nd:ASL crystal and the availability of optimally-cooled Nd^{3+}-doped crystals allows one to have a simple thermal management. Moreover, the fractional heat loading for Nd lasers is clearly better than that for Tm lasers operating at 2.3 µm. This implicates that, in our case, the heating of the Tm:$LiYF_4$ crystal remains moderate even at high applied levels of the primary pump. Indeed, when the Tm:$LiYF_4$ crystal is aligned to be pumped at 1 µm in σ-polarization, the temperature gradient measured with respect to the surface of this crystal is only 15 °C. In the absence of laser emission at 2.3 µm, this gradient is 7 °C.

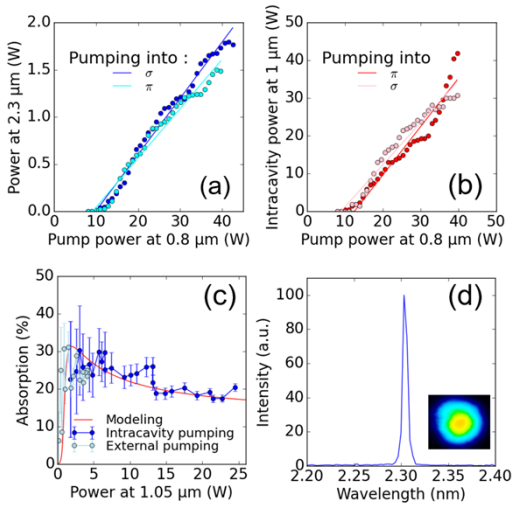

Fig. 2. Tm:$LiYF_4$ laser with intracavity upconversion pumping by a Nd:ASL laser: (a) output power at 2.3 μm and (b) intracavity power at 1.05 μm accounting for a roundtrip pass through the Tm-crystal. The polarization of the 1.05 μm radiation corresponds to π or σ with a slope efficiency of the 2.3-μm laser being 30% and 22%, respectively (versus the absorbed pump power at 1.05 μm); (c) absorption of the Tm: $LiYF_4$ crystal at 1.05 μm when pumping into σ polarization; (d) laser spectrum at 2.3 μm (π-polarized emission), *inset* – a typical far-field profile of the 2.3-μm laser.

A key point to consider in intracavity laser pumping concerns the strong interplay between the Tm:$LiYF_4$ absorption and the 1.05-μm intracavity power, since the former effect can be seen as an intracavity loss for the Nd laser. This can be easily verified using the fact that the ESA cross-sections for Tm^{3+} ions in $LiYF_4$ are different for σ and π polarizations. The crystal can be 90° rotated to choose the pump polarization state. When orienting the Tm:$LiYF_4$ crystal for pumping in π polarization, the absorption at 1.05 μm drastically decreases and so does the intracavity loss for the Nd laser. The measured absorption at 1.05 μm indeed drops from 20% down to only 8% per pass and the intracavity power increases up to 40 W in this latter configuration (for a laser-diode power of 42 W). *In fine*, these two effects counteract each other and the output power at 2.3 μm marginally drops to 1.51 W for pumping into π polarization. Thus, despite the strong absorption differences between π and σ polarizations, their effect on laser emission at 2.3 μm is quite limited. These results spotlight the adaptability of the intracavity pumping scheme to fit the absorption of the Tm:$LiYF_4$ crystal. As the 1.05 μm pump absorption efficiency decreases, the intracavity power at this wavelength tends to increase, so that the tolerance to the Tm absorption is significantly improved. This large adaptability to the Tm absorption is a key advantage of the intracavity upconversion pumping scheme vs. the "extracavity" one. Indeed, the latter scheme is very sensitive to pump intensity variations and Tm^{3+} doping concentration, and the choice of the Tm^{3+}-based laser crystal is quite critical. It is also interesting to consider that in the case of "extracavity" pumping [14,15,22], the pump intensity must be maximized to boost the pump absorption efficiency. In the case of intracavity pumping, the intensity level is not a matter anymore, since, first, the maximum absorption is largely exceeded, Fig. 2(c), and second, small ESA cross-sections are compensated by higher intracavity power. This adaptability has another consequence. Considering the broad wavelength tunability of Nd:ASL [21], when the polarization of the 1.05 μm emission corresponds to σ in the Tm:$LiYF_4$ crystal, the Nd laser wavelength experiences a slight blue shift thus matching weaker absorption of Tm^{3+} ions, see Fig. 1(b). The corresponding variation of the central wavelength is 0.7 nm. The spectrum around 1051 nm and so the pump absorption at this wavelength are thus sensitive to pump variation and alignment. This self-adaptation in the optimization process of the 2.3-μm laser could create sharp variations in the absorption curve at 1.05 μm. Such variations are visible in the plot of 1.05-μm intracavity power versus pump power at 0.8 μm, see Fig. 2(c), whereas the effect on the 2.3-μm laser performance is limited. In any case, no temporal instability or shift in the 1.05-μm laser wavelength is observed.

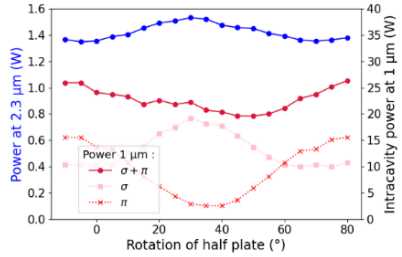

Fig. 3. Tm:$LiYF_4$ laser with intracavity upconversion pumping by a Nd:ASL laser: output power at 2.3 μm and the intracavity power at 1.05 μm versus the angle of rotation of an intracavity half-wave plate. Pumping into π and σ polarizations corresponds to the rotation angles of 0° and 45°, respectively.

The adaptability of the intracavity pumping is also observed by introducing a half-wave plate before the intracavity lens (f = 80 mm) in the 1051-nm Nd laser cavity. In this case, we have measured an unchanged linear polarization in the Nd:ASL crystal and an adjustable linear polarization of the 1.05 μm intracavity radiation addressing a combination of absorption features of Tm:$LiYF_4$ for two orthogonal eigen polarization states. The optical axis of the Tm:$LiYF_4$ crystal and the axis of the waveplate overlap for a rotation angle of 0°. Rotating the 1.05 μm polarization tends to change the intracavity power at 1.05 μm by 25% in the worst case because of a strong ESA anisotropy for Tm^{3+} ions in $LiYF_4$. At the same time, the 2.3 μm power increases by 19%. Note that the variation of thermal lensing due to the power variations at 1.05 μm and 2.3 μm is not compensated during the waveplate rotation.

Another key issue in the intracavity pumping scheme where the 1.05-μm laser intensity is very high and so the ESA at this wavelength, concerns the population of higher-lying excited states of Tm^{3+} ions. Indeed, at such high levels of intracavity laser intensity at 1.05 μm in the Tm:$LiYF_4$ crystal, intense visible fluorescence at the wavelengths of 300 -500 nm is observed as seen in Fig. 4(b). The possibility of a significant ESA from the $^3H_4$ level is not negligible, and one may wonder whether this effect can limit the 2.3-μm laser performance. We have measured the Tm^{3+} fluorescence with and without 2.3 μm laser emission to obtain information about the population of the $^1D_2$, $^1G_4$ and $^3H_4$ levels. Figure 4(a) shows the correspondences between the fluorescence wavelengths and the Tm^{3+} transitions and indicates the branching ratios (in percents) and the fluorescence lifetimes of the emitting states, after [14,23]. The main fluorescence peaks are assigned. To estimate the population of these levels, we assume that the power (*P*) collected

by the spectrometer is defined as $P \propto \beta \frac{hc}{\lambda \tau} nNV$, where, for a given transition, β is its branching ratio, λ is the central wavelength, τ is the lifetime of the emitting state, n is its fractional population in percents, N is the Tm^{3+} ion density expressed in cm^{-3}, and V is the volume of the pumped region. This equation is a proportional relation, so it gives only the ratio of populations between several excited states. However, the population of the $^3H_4$ level under laser conditions at 2.3 µm is known from the condition "gain is equal to losses". The fractional population of the $^3H_4$ level is estimated to be about 1%. Thus, by measuring the intensity ratios between several fluorescence lines, as well as those with and without laser action at 2.3 µm, one can calculate the populations of higher-lying manifolds. Under laser conditions, the fractional $^1D_2$, $^1G_4$ and $^3H_4$ populations are 1×10^{-4} %, 0.03% and 1%, respectively. Without laser operation at 2.3 µm, they amount to 0.08%, 0.3% and 10%, respectively. Although the population of the $^1G_4$ level filled by an ESA process from the $^3H_4$ level is not negligible without laser action at 2.3 µm, its population decreases significantly under laser operation, reducing its potential negative impact. This decrease is due to the emptying of the $^3H_4$ manifold by laser emission.

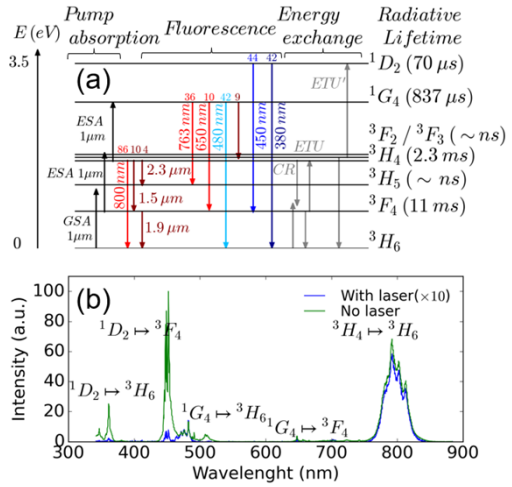

Fig. 4. (a) A detailed energy-level scheme of Tm^{3+} ions with assigned florescence transitions. The values above the transitions correspond to the branching ratios in percents. ETU and ETU': energy-transfer upconversion from the $^3F_4$ and $^3H_4$ levels, respectively; (b) Spectra of visible fluorescence from the Tm:$LiYF_4$ crystal for 20 W of intracavity power at 1.05 µm with and without laser at 2.3 µm.

In conclusion, the results obtained in the present work highlight the important potential of the intracavity pumping scheme of a 2.3-µm Tm:$LiYF_4$ laser using the advantages of the Nd-laser technology. We show that the adaptability of the intracavity pumping scheme to the excited-state absorption of Tm^{3+} ions plays an important role in boosting the laser performance. As the intracavity power adapts itself to the absorption of the intracavity pump radiation at 1.05 µm, the problem of weak absorption in "extracavity" upconversion pumped Tm:$LiYF_4$ crystals does not appear anymore as a limitation. This is a key advantage of the intracavity upconversion pumping scheme. The output power obtained in the present work which is a first proof-of-concept is already competitive with the previously reported directly diode-pumped 2.3-µm Tm:$LiYF_4$ lasers. Moreover, compared to the latter pumping scheme, the heating of the Tm-crystal is relatively weak and does not represent any limitation for power scaling, which opens interesting new perspectives for high-power lasers at 2.3 µm based on thulium technology.

Funding. French Agence Nationale de la Recherche (ANR, project SPLENDID2, ANR-19-CE08-0028); Région Normandie (Chaire d'excellence "RELANCE").

Disclosures. The authors declare no conflicts of interest.

Data availability. Data underlying the results presented in this paper are not publicly available at this time but may be obtained from the authors upon reasonable request.

References

1. G. G. Taylor, D. Morozov, N. R. Gemmell, K. Erotokritou, S. Miki, H. Terai, and R. H. Hadfield, Opt. Express **27**, 38147 (2019).
2. F. J. McAleavey, J. O'Gorman, J. F. Donegan, B. D. MacCraith, J. Hegarty and G. Maze, IEEE J. Sel. Top. Quantum Electron. **3**, 1103 (1997).
3. V. Petrov, Progr. Quantum Electron. **42**, 1 (2015).
4. D. A. Yarekha, G. Glastre, A. Perona, Y. Rouillard, F. Genty, E. M. Skouri, G. Boissier, P. Grech, A. Joullié, C. Alibert, and A. N. Baranov, Electron. Lett. **36**, 537 (2000).
5. A. Salhi, Y. Rouillard, A. Pérona, P. Grech, M. Garcia, and C. Sirtori, Semicond. Sci. Technol. **19**, 260 (2004)
6. I. Moskalev, S. Mirov, M. Mirov, S. Vasilyev, V. Smolski, A. Zakrevskiy, and V. Gapontsev, Opt. Mater. Express **7**, 2636 (2017).
7. J. Caird, L. DeShazer, and J. Nella, IEEE J. Quantum Electron. **11**, 874 (1975).
8. P. Loiko, R. Soulard, L. Guillemot, G. Brasse, J.-L. Doualan, A. Braud, A. Tyazhev, A. Hideur, F. Druon, and P. Camy. IEEE J. Quantum Electron. **55**, 1700212 (2019).
9. E. Kifle, P. Loiko, L. Guillemot, J.-L. Doualan, F. Starecki, A. Braud, T. Georges, J. Rouvillain, and P. Camy, Appl. Opt. **59**, 7530 (2020).
10. X. Yu, K. Eremeev, Z. Pan, P. Loiko, H. Chu, H. Pan, S. Zhao, A. Braud, P. Camy, and D. Li, Opt. Lett. **48**, 6404 (2023).
11. X. Yu, Z. Pan, H. Chu, H. Pan, S. Zhao, and D. Li, Opt. Express **31**, 26368 (2023).
12. H. Dupont, L. Guillemot, P. Loiko, R. M. Solé, X. Mateos, M. Aguiló, F. Díaz, A. Braud, P. Camy, P. Georges, and F. Druon, Opt. Express **31**, 34201 (2023)
13. A. Tyazhev, F. Starecki, S. Cozic, P. Loiko, L. Guillemot, A. Braud, F. Joulain, M. Tang, T. Godin, A. Hideur, and P. Camy, Opt. Lett. **45**, 5788 (2020).
14. L. Guillemot, P. Loiko, R. Soulard, A. Braud, J.-L. Doualan, A. Hideur, R. Moncorgé, and P. Camy, Opt. Lett. **44**, 4071 (2019).
15. H. Dupont, L. Guillemot, P. Loiko, A. Braud, J.-L. Doualan, P. Camy, P. Georges, and F. Druon, Opt. Express **30**, 32141 (2022).
16. R. L. Kohn, C. V. Shank, E. P. Ippen, and A. Dienes, Opt. Commun. **3**, 177 (1971).
17. S. So, J. I. Mackenzie, D. P. Shepherd, W. A. Clarkson, J. G. Betterton, E. K. Gorton, and J. A. C. Terry, Opt. Express **14**, 10481 (2006).
18. R. C. Stoneman and L. Esterowitz, Opt. Lett. **17**, 736 (1992).
19. E. Herault, F. Balembois, P. Georges, and T. Georges, Opt. Lett. **33**, 1632 (2008).
20. Z. Chen, Z. Huang, M. He, T. Xu, Q. Na, L. Zhang, Y. Li, C. Xu, X. Xu, J. Xu, and D. Fan, Appl. Phys. Express **13**, 032004 (2020).
21. W. Lin, C. Huang, S. Li, S. Tao, G. Chen, M. Xu, C. Zhao, Q. Fang, X. Ye, and Y. Hang, Infrared Phys. Technol. **136**, 105066 (2024).
22. Y. Morova, M. Tonelli, V. Petrov, and A. Sennaroglu, Opt. Lett. **45**, 931 (2020).
23. B. M. Walsh, N. P. Barnes, and B. Di Bartolo, J. Appl. Phys. **83**, 2772 (1998).

Full References

1. G. G. Taylor, D. Morozov, N. R. Gemmell, K. Erotokritou, S. Miki, H. Terai, and R. H. Hadfield, “Photon counting LIDAR at 2.3 µm wavelength with superconducting nanowires,” Opt. Express **27**(26), 38147-38158 (2019).
2. F. J. McAleavey, J. O'Gorman, J. F. Donegan, B. D. MacCraith, J. Hegarty and G. Maze, “Narrow linewidth, tunable Tm^{3+}-doped fluoride fiber laser for optical-based hydrocarbon gas sensing,” IEEE J. Sel. Top. Quantum Electron. **3**(4), 1103-1111 (1997).
3. V. Petrov, “Frequency down-conversion of solid-state laser sources to the mid-infrared spectral range using non-oxide nonlinear crystals,” Progr. Quantum Electron. **42**, 1–106 (2015).
4. D. A. Yarekha, G. Glastre, A. Perona, Y. Rouillard, F. Genty, E. M. Skouri, G. Boissier, P. Grech, A. Joullié, C. Alibert, and A. N. Baranov, "High temperature GaInSbAs/GaAlSbAs quantum well singlemode continuous wave lasers emitting near 2.3 µm," Electronics Letters **36**(6), 537–539 (2000).
5. A. Salhi, Y. Rouillard, A. Pérona, P. Grech, M. Garcia, and C. Sirtori, "Low-threshold GaInAsSb/AlGaAsSb quantum well laser diodes emitting near 2.3 µm," Semicond. Sci. Technol. 19(2), 260–262 (2004)
6. I. Moskalev, S. Mirov, M. Mirov, S. Vasilyev, V. Smolski, A. Zakrevskiy, and V. Gapontsev, “Ultrafast middle-IR lasers and amplifiers based on polycrystalline Cr:ZnS and Cr:ZnSe,” Opt. Mater. Express 7(7), 2636-2650 (2017).
7. J. Caird, L. DeShazer, and J. Nella, “Characteristics of room-temperature 2.3-µm laser emission from Tm3+ in YAG and YAlO3,” IEEE J. Quantum Electron. 11(11), 874-881 (1975).
8. P. Loiko, R. Soulard, L. Guillemot, G. Brasse, J.-L. Doualan, A. Braud, A. Tyazhev, A. Hideur, F. Druon, and P. Camy. Efficient Tm:$LiYF_4$ lasers at ∼2.3 μm: Effect of energy-transfer upconversion,” IEEE J. Quantum Electron. **55**(6), 1700212-1–12 (2019).
9. E. Kifle, P. Loiko, L. Guillemot, J.-L. Doualan, F. Starecki, A. Braud, T. Georges, J. Rouvillain, and P. Camy, "Watt-level diode-pumped thulium lasers around 2.3 µm," Appl. Opt. **59**(25), 7530-7539 (2020).
10. X. Yu, K. Eremeev, Z. Pan, P. Loiko, H. Chu, H. Pan, S. Zhao, A. Braud, P. Camy, and D. Li, "Six-watt diode-pumped Tm:$GdVO_4$ laser at 2.29 µm," Opt. Lett., OL **48**(24), 6404–6407 (2023).
11. X. Yu, Z. Pan, H. Chu, H. Pan, S. Zhao, and D. Li, "Diode-pumped efficient high-power cascade Tm:$GdVO_4$ laser simultaneously operating at ∼2 µm and ∼2.3 µm," Opt. Express **31**(16), 26368 (2023).
12. H. Dupont, L. Guillemot, P. Loiko, R. M. Solé, X. Mateos, M. Aguiló, F. Díaz, A. Braud, P. Camy, P. Georges, and F. Druon, "Cascade laser optimization for $^3H_4 \rightarrow {}^3H_5$ and $^3F_4 \rightarrow {}^3H_6$ sequent transitions in Tm^{3+}-doped materials," Opt. Express **31**, 34201-34212 (2023)
13. A. Tyazhev, F. Starecki, S. Cozic, P. Loiko, L. Guillemot, A. Braud, F. Joulain, M. Tang, T. Godin, A. Hideur, and P. Camy, "Watt-level efficient 2.3 µm thulium fluoride fiber laser," Opt. Lett. 45(20), 5788-5791 (2020).
14. L. Guillemot, P. Loiko, R. Soulard, A. Braud, J.-L. Doualan, A. Hideur, R. Moncorgé, and P. Camy, "Thulium laser at ∼2.3 µm based on upconversion pumping," Opt. Lett. **44**(16), 4071-4074 (2019).
15. H. Dupont, L. Guillemot, P. Loiko, A. Braud, J.-L. Doualan, P. Camy, P. Georges, and F. Druon, "Dual-wavelength-pumping of mid-infrared Tm:YLF laser at 2.3 µm: demonstration of pump seeding and recycling processes," Opt. Express **30**(18), 32141-32150 (2022).
16. R. L. Kohn, C. V. Shank, E. P. Ippen, and A. Dienes, "An intracavity-pumped CW dye laser," Optics Communications 3(3), 177–178 (1971).
17. S. So, J. I. Mackenzie, D. P. Shepherd, W. A. Clarkson, J. G. Betterton, E. K. Gorton, and J. A. C. Terry, "Intra-cavity side-pumped Ho:YAG laser," Opt. Express **14**(22), 10481 (2006).
18. R. C. Stoneman and L. Esterowitz, "Intracavity-pumped 209-µm Ho:YAG laser," Opt. Lett. **17**(10), 736 (1992).
19. E. Herault, F. Balembois, P. Georges, and T. Georges, "1064 nm Nd:YVO4 laser intracavity pumped at 912 nm and sum-frequency mixing for an emission at 491 nm," Opt. Lett., OL 33(14), 1632–1634 (2008).
20. Z. Chen, Z. Huang, M. He, T. Xu, Q. Na, L. Zhang, Y. Li, C. Xu, X. Xu, J. Xu, and D. Fan, "Highly efficient continuous-wave and mode-locking operation of a diode-pumped Nd:ASL disordered crystal laser," Appl. Phys. Express **13**(3), 032004 (2020).
21. W. Lin, C. Huang, S. Li, S. Tao, G. Chen, M. Xu, C. Zhao, Q. Fang, X. Ye, and Y. Hang, "Tunable laser operations on Nd-doped strontium and lanthanum aluminate crystals," Infrared Physics & Technology 136, 105066 (2024).
22. Y. Morova, M. Tonelli, V. Petrov, and A. Sennaroglu, "Upconversion pumping of a 2.3 µm Tm^{3+}:KY_3F_{10} laser with a 1064 nm ytterbium fiber laser," Opt. Lett. **45**(4), 931 (2020).
23. B. M. Walsh, N. P. Barnes, and B. Di Bartolo, "Branching ratios, cross sections, and radiative lifetimes of rare earth ions in solids: Application to Tm3+ and Ho3+ ions in LiYF4," Journal of Applied Physics **83**(5), 2772–2787 (1998).